Measurements of Baryon Pair Decays of χ_{cJ} Mesons

M. Ablikim[1], M. N. Achasov[6], O. Albayrak[3], D. J. Ambrose[39], F. F. An[1], Q. An[40], J. Z. Bai[1], Y. Ban[26], J. Becker[2], J. V. Bennett[16], M. Bertani[17A], J. M. Bian[38], E. Boger[19,a], O. Bondarenko[20], I. Boyko[19], R. A. Briere[3], V. Bytev[19], X. Cai[1], O. Cakir[34A], A. Calcaterra[17A], G. F. Cao[1], S. A. Cetin[34B], J. F. Chang[1], G. Chelkov[19,a], G. Chen[1], H. S. Chen[1], J. C. Chen[1], M. L. Chen[1], S. J. Chen[24], X. Chen[26], Y. B. Chen[1], H. P. Cheng[14], Y. P. Chu[1], D. Cronin-Hennessy[38], H. L. Dai[1], J. P. Dai[1], D. Dedovich[19], Z. Y. Deng[1], A. Denig[18], I. Denysenko[19,b], M. Destefanis[43A,43C], W. M. Ding[28], Y. Ding[22], L. Y. Dong[1], M. Y. Dong[1], S. X. Du[46], J. Fang[1], S. S. Fang[1], L. Fava[43B,43C], C. Q. Feng[40], R. B. Ferroli[17A], P. Friedel[2], C. D. Fu[1], Y. Gao[33], C. Geng[40], K. Goetzen[7], W. X. Gong[1], W. Gradl[18], M. Greco[43A,43C], M. H. Gu[1], Y. T. Gu[9], Y. H. Guan[36], A. Q. Guo[25], L. B. Guo[23], T. Guo[23], Y. P. Guo[25], Y. L. Han[1], F. A. Harris[37], K. L. He[1], M. He[1], Z. Y. He[25], T. Held[2], Y. K. Heng[1], Z. L. Hou[1], C. Hu[23], H. M. Hu[1], J. F. Hu[35], T. Hu[1], G. M. Huang[4], G. S. Huang[40], J. S. Huang[12], L. Huang[1], X. T. Huang[28], Y. Huang[24], Y. P. Huang[1], T. Hussain[42], C. S. Ji[40], Q. Ji[1], Q. P. Ji[25], X. B. Ji[1], X. L. Ji[1], L. L. Jiang[1], X. S. Jiang[1], J. B. Jiao[28], Z. Jiao[14], D. P. Jin[1], S. Jin[1], F. F. Jing[33], N. Kalantar-Nayestanaki[20], M. Kavatsyuk[20], B. Kopf[2], M. Kornicer[37], W. Kuehn[35], W. Lai[1], J. S. Lange[35], M. Leyhe[2], C. H. Li[1], Cheng Li[40], Cui Li[40], D. M. Li[46], F. Li[1], G. Li[1], H. B. Li[1], J. C. Li[1], K. Li[10], Lei Li[1], Q. J. Li[1], S. L. Li[1], W. D. Li[1], W. G. Li[1], X. L. Li[28], X. N. Li[1], X. Q. Li[25], X. R. Li[27], Z. B. Li[32], H. Liang[40], Y. F. Liang[30], Y. T. Liang[35], G. R. Liao[33], X. T. Liao[1], D. Lin[11], B. J. Liu[1], C. L. Liu[3], C. X. Liu[1], F. H. Liu[29], Fang Liu[1], Feng Liu[4], H. Liu[1], H. B. Liu[9], H. H. Liu[13], H. M. Liu[1], H. W. Liu[1], J. P. Liu[44], K. Liu[33], K. Y. Liu[22], Kai Liu[36], P. L. Liu[28], Q. Liu[36], S. B. Liu[40], X. Liu[21], Y. B. Liu[25], Z. A. Liu[1], Zhiqiang Liu[1], Zhiqing Liu[1], H. Loehner[20], G. R. Lu[12], H. J. Lu[14], J. G. Lu[1], Q. W. Lu[29], X. R. Lu[36], Y. P. Lu[1], C. L. Luo[23], M. X. Luo[45], T. Luo[37], X. L. Luo[1], M. Lv[1], C. L. Ma[36], F. C. Ma[22], H. L. Ma[1], Q. M. Ma[1], S. Ma[1], T. Ma[1], X. Y. Ma[1], F. E. Maas[11], M. Maggiora[43A,43C], Q. A. Malik[42], Y. J. Mao[26], Z. P. Mao[1], J. G. Messchendorp[20], J. Min[1], T. J. Min[1], R. E. Mitchell[16], X. H. Mo[1], C. Morales Morales[11], N. Yu. Muchnoi[6], H. Muramatsu[39], Y. Nefedov[19], C. Nicholson[36], I. B. Nikolaev[6], Z. Ning[1], S. L. Olsen[27], Q. Ouyang[1], S. Pacetti[17B], J. W. Park[27], M. Pelizaeus[2], H. P. Peng[40], K. Peters[7], J. L. Ping[23], R. G. Ping[1], R. Poling[38], E. Prencipe[18], M. Qi[24], S. Qian[1], C. F. Qiao[36], L. Q. Qin[28], X. S. Qin[1], Y. Qin[26], Z. H. Qin[1], J. F. Qiu[1], K. H. Rashid[42], G. Rong[1], X. D. Ruan[9], A. Sarantsev[19,c], B. D. Schaefer[16], M. Shao[40], C. P. Shen[37,d], X. Y. Shen[1], H. Y. Sheng[1], M. R. Shepherd[16], X. Y. Song[1], S. Spataro[43A,43C], B. Spruck[35], D. H. Sun[1], G. X. Sun[1], J. F. Sun[12], S. S. Sun[1], Y. J. Sun[40], Y. Z. Sun[1], Z. J. Sun[1], Z. T. Sun[40], C. J. Tang[30], X. Tang[1], I. Tapan[34C], E. H. Thorndike[39], D. Toth[38], M. Ullrich[35], G. S. Varner[37], B. Q. Wang[26], D. Wang[26], D. Y. Wang[26], K. Wang[1], L. L. Wang[1], L. S. Wang[1], M. Wang[28], P. Wang[1], P. L. Wang[1], Q. J. Wang[1], S. G. Wang[26], X. F. Wang[33], X. L. Wang[40], Y. F. Wang[1], Z. Wang[1], Z. G. Wang[1], Z. Y. Wang[1], D. H. Wei[8], J. B. Wei[26], P. Weidenkaff[18], Q. G. Wen[40], S. P. Wen[1], M. Werner[35], U. Wiedner[2], L. H. Wu[1], N. Wu[1], S. X. Wu[40], W. Wu[25], Z. Wu[1], L. G. Xia[33], Z. J. Xiao[23], Y. G. Xie[1], Q. L. Xiu[1], G. F. Xu[1], G. M. Xu[26], Q. J. Xu[10], Q. N. Xu[36], X. P. Xu[31], Z. R. Xu[40], F. Xue[4], Z. Xue[1], L. Yan[40], W. B. Yan[40], Y. H. Yan[15], H. X. Yang[1], Y. Yang[4], Y. X. Yang[8], H. Ye[1], M. Ye[1], M. H. Ye[5], B. X. Yu[1], C. X. Yu[25], H. W. Yu[26], J. S. Yu[21], S. P. Yu[28], C. Z. Yuan[1], Y. Yuan[1], A. A. Zafar[42], A. Zallo[17A], Y. Zeng[15], B. X. Zhang[1], B. Y. Zhang[1], C. Zhang[24], C. C. Zhang[1], D. H. Zhang[1], H. H. Zhang[32], H. Y. Zhang[1],

J. Q. Zhang[1], J. W. Zhang[1], J. Y. Zhang[1], J. Z. Zhang[1], R. Zhang[36], S. H. Zhang[1], X. J. Zhang[1], X. Y. Zhang[28], Y. Zhang[1], Y. H. Zhang[1], Z. P. Zhang[40], Z. Y. Zhang[44], Zhenghao Zhang[4], G. Zhao[1], H. S. Zhao[1], J. W. Zhao[1], K. X. Zhao[23], Lei Zhao[40], Ling Zhao[1], M. G. Zhao[25], Q. Zhao[1], Q. Z. Zhao[9], S. J. Zhao[46], T. C. Zhao[1], Y. B. Zhao[1], Z. G. Zhao[40], A. Zhemchugov[19,a], B. Zheng[41], J. P. Zheng[1], Y. H. Zheng[36], B. Zhong[23], Z. Zhong[9], L. Zhou[1], X. K. Zhou[36], X. R. Zhou[40], C. Zhu[1], K. Zhu[1], K. J. Zhu[1], S. H. Zhu[1], X. L. Zhu[33], Y. C. Zhu[40], Y. M. Zhu[25], Y. S. Zhu[1], Z. A. Zhu[1], J. Zhuang[1], B. S. Zou[1], J. H. Zou[1]

(BESIII Collaboration)

[1] *Institute of High Energy Physics, Beijing 100049, People's Republic of China*
[2] *Bochum Ruhr-University, 44780 Bochum, Germany*
[3] *Carnegie Mellon University, Pittsburgh, Pennsylvania 15213, USA*
[4] *Central China Normal University, Wuhan 430079, People's Republic of China*
[5] *China Center of Advanced Science and Technology, Beijing 100190, People's Republic of China*
[6] *G.I. Budker Institute of Nuclear Physics SB RAS (BINP), Novosibirsk 630090, Russia*
[7] *GSI Helmholtzcentre for Heavy Ion Research GmbH, D-64291 Darmstadt, Germany*
[8] *Guangxi Normal University, Guilin 541004, People's Republic of China*
[9] *GuangXi University, Nanning 530004, People's Republic of China*
[10] *Hangzhou Normal University, Hangzhou 310036, People's Republic of China*
[11] *Helmholtz Institute Mainz, J.J. Becherweg 45,D 55099 Mainz,Germany*
[12] *Henan Normal University, Xinxiang 453007, People's Republic of China*
[13] *Henan University of Science and Technology, Luoyang 471003, People's Republic of China*
[14] *Huangshan College, Huangshan 245000, People's Republic of China*
[15] *Hunan University, Changsha 410082, People's Republic of China*
[16] *Indiana University, Bloomington, Indiana 47405, USA*
[17] *(A)INFN Laboratori Nazionali di Frascati, I-00044, Frascati, Italy; (B)INFN and University of Perugia, I-06100, Perugia, Italy*
[18] *Johannes Gutenberg University of Mainz, Johann-Joachim-Becher-Weg 45, 55099 Mainz, Germany*
[19] *Joint Institute for Nuclear Research, 141980 Dubna, Moscow region, Russia*
[20] *KVI, University of Groningen, 9747 AA Groningen, The Netherlands*
[21] *Lanzhou University, Lanzhou 730000, People's Republic of China*
[22] *Liaoning University, Shenyang 110036, People's Republic of China*
[23] *Nanjing Normal University, Nanjing 210023, People's Republic of China*
[24] *Nanjing University, Nanjing 210093, People's Republic of China*
[25] *Nankai University, Tianjin 300071, People's Republic of China*
[26] *Peking University, Beijing 100871, People's Republic of China*
[27] *Seoul National University, Seoul, 151-747 Korea*
[28] *Shandong University, Jinan 250100, People's Republic of China*
[29] *Shanxi University, Taiyuan 030006, People's Republic of China*
[30] *Sichuan University, Chengdu 610064, People's Republic of China*
[31] *Soochow University, Suzhou 215006, People's Republic of China*
[32] *Sun Yat-Sen University, Guangzhou 510275, People's Republic of China*
[33] *Tsinghua University, Beijing 100084, People's Republic of China*

[34] *(A)Ankara University, Dogol Caddesi, 06100 Tandogan, Ankara, Turkey; (B)Dogus University, 3722 Istanbul, Turkey; (C)Uludag University, 16059 Bursa, Turkey*
[35] *Universitaet Giessen, 35392 Giessen, Germany*
[36] *University of Chinese Academy of Sciences, Beijing 100049, People's Republic of China*
[37] *University of Hawaii, Honolulu, Hawaii 96822, USA*
[38] *University of Minnesota, Minneapolis, Minnesota 55455, USA*
[39] *University of Rochester, Rochester, New York 14627, USA*
[40] *University of Science and Technology of China, Hefei 230026, People's Republic of China*
[41] *University of South China, Hengyang 421001, People's Republic of China*
[42] *University of the Punjab, Lahore-54590, Pakistan*
[43] *(A)University of Turin, I-10125, Turin, Italy; (B)University of Eastern Piedmont, I-15121, Alessandria, Italy; (C)INFN, I-10125, Turin, Italy*
[44] *Wuhan University, Wuhan 430072, People's Republic of China*
[45] *Zhejiang University, Hangzhou 310027, People's Republic of China*
[46] *Zhengzhou University, Zhengzhou 450001, People's Republic of China*

[a] *Also at the Moscow Institute of Physics and Technology, Moscow 141700, Russia*
[b] *On leave from the Bogolyubov Institute for Theoretical Physics, Kiev 03680, Ukraine*
[c] *Also at the PNPI, Gatchina 188300, Russia*
[d] *Present address: Nagoya University, Nagoya 464-8601, Japan*

(Dated: November 13, 2012)

Abstract

Using 106 million ψ' decays collected with the BESIII detector at the BEPCII, three decays of χ_{cJ} ($J = 0, 1, 2$) with a baryon pair ($\Lambda\bar{\Lambda}$, $\Sigma^0\bar{\Sigma}^0$, $\Sigma^+\bar{\Sigma}^-$) in the final state have been studied. The branching fractions are measured to be $B(\chi_{c0,1,2} \to \Lambda\bar{\Lambda}) = (33.3 \pm 2.0 \pm 2.6) \times 10^{-5}$, $(12.2 \pm 1.1 \pm 1.1) \times 10^{-5}$, $(20.8 \pm 1.6 \pm 2.3) \times 10^{-5}$; $B(\chi_{c0,1,2} \to \Sigma^0\bar{\Sigma}^0)$ =$(47.8 \pm 3.4 \pm 3.9) \times 10^{-5}$, $(3.8 \pm 1.0 \pm 0.5) \times 10^{-5}$, $(4.0 \pm 1.1 \pm 0.5) \times 10^{-5}$; and $B(\chi_{c0,1,2} \to \Sigma^+\bar{\Sigma}^-)$ = $(45.4 \pm 4.2 \pm 3.0) \times 10^{-5}$, $(5.4 \pm 1.5 \pm 0.5) \times 10^{-5}$, $(4.9 \pm 1.9 \pm 0.7) \times 10^{-5}$, where the first error is statistical and the second is systematic. Upper limits on the branching fractions for the decays of $\chi_{c1,2} \to \Sigma^0\bar{\Sigma}^0$, $\Sigma^+\bar{\Sigma}^-$, are set up to be $B(\chi_{c1} \to \Sigma^0\bar{\Sigma}^0) < 6.2 \times 10^{-5}$, $B(\chi_{c2} \to \Sigma^0\bar{\Sigma}^0) < 6.5 \times 10^{-5}$, $B(\chi_{c1} \to \Sigma^+\bar{\Sigma}^-) < 8.7 \times 10^{-5}$ and $B(\chi_{c2} \to \Sigma^+\bar{\Sigma}^-) < 8.8 \times 10^{-5}$ at the 90% confidence level.

PACS numbers: 12.38.Qk, 13.25.Gv, 14.20.Gk, 14.40.Gx

I. INTRODUCTION

In the standard quark model, χ_{cJ} (J = 0, 1, 2), mesons are $c\bar{c}$ states in an L = 1 configuration. Experimental studies on χ_{cJ} decay properties are essential to test perturbative Quantum Chromodynamics (QCD) models and QCD-based calculations. The importance of the color octet mechanism (COM) for χ_{cJ} decays has been pointed out for many years [1], and theoretical predictions of two-body exclusive decays have been made based on it. The predictions of COM theory for some χ_{cJ} decays into baryon pairs ($B\bar{B}$) (for example, the branching fractions of $\chi_{cJ} \to \Lambda\bar{\Lambda}$) disagree with measured values. Although many experimental results on χ_{cJ} exclusive decays have been reported [2–4], many decay modes of $\chi_{cJ} \to B\bar{B}$ have not been observed yet, and other modes are measured with poor precision. For further testing of the COM in the decays of the P-wave charmonia, measurements of other baryon pair decays of χ_{cJ}, such as $\chi_{cJ} \to \Lambda\bar{\Lambda}$, $\Sigma^0\bar{\Sigma}^0$ and $\Sigma^+\bar{\Sigma}^-$, are desired.

In addition, measurements of $\chi_{c0} \to B\bar{B}$ are helpful for understanding the helicity selection rule (HSR) [5], which prohibits χ_{c0} decays into baryon-antibaryon pairs. Actually the measured branching ratios for $\chi_{c0} \to B\bar{B}$ do not vanish, for example $\chi_{c0} \to p\bar{p}$ [6], demonstrating a strong violation of HSR in charmonium decays. Therefore, it is important to measure the decays of $\chi_{c0} \to B\bar{B}$ to provide additional tests of the HSR.

While χ_{cJ} mesons are not produced directly in e^+e^- annihilations, the large branching fractions of $\psi' \to \gamma\chi_{cJ}$ make e^+e^- collisions at the ψ' energy a very clean environment for χ_{cJ} investigation. In this paper, the results of two-body decays of $\chi_{cJ} \to \Lambda\bar{\Lambda}$, $\Sigma^0\bar{\Sigma}^0$ and $\Sigma^+\bar{\Sigma}^-$ final states are presented. We report the most precise measurements of the following three modes: $\Lambda\bar{\Lambda}$, $\Sigma^0\bar{\Sigma}^0$ and $\Sigma^+\bar{\Sigma}^-$. This analysis is based on 106 million ψ' events [7] collected with BESIII at the BEPCII. A sample of 44 pb^{-1} of data taken at $\sqrt{s}$ =3.65 GeV is used for continuum background study.

II. BESIII DETECTOR AND MONTE CARLO SIMULATION

BEPCII is a double-ring e^+e^- collider with designed to reach peak luminosity of about $0.6 \times 10^{33}\ \mathrm{cm^{-2}s^{-1}}$ at the peak energy of $\psi(3770)$. The cylindrical core of the BESIII detector consists of a helium-based main drift chamber (MDC), a plastic scintillator time-of-flight system (TOF), and a CsI(Tl) electromagnetic calorimeter (EMC), which are all enclosed in a superconducting solenoidal magnet providing a 1.0 T magnetic field. The solenoid is supported by an octagonal flux-return yoke with resistive plate counter muon identifier modules interleaved with steel. The acceptance for charged particles and photons is 93% over 4π stereo angle, and the charged-particle momentum and photon energy resolutions at 1 GeV are 0.5% and 2.5%, respectively. The detector is described in more detail in [8].

The BESIII detector is modeled with a Monte Carlo (MC) simulation based on GEANT4 [9, 10]. The ψ' resonance is produced with KKMC [11], while the subsequent decays are generated with EVTGEN [12] according to the branching fractions provided by the Particle Data Group (PDG) [6], and the remaining unknown decay modes are generated with LUNDCHARM [13].

III. EVENT SELECTION

The investigated final states include Λ ($\bar{\Lambda}$), p ($\bar{p}$), or neutral π^0 mesons, and a radiative photon from the decay $\psi' \to \gamma\chi_{cJ}$, where Λ ($\bar{\Lambda}$) decays to $\pi^- p$ ($\pi^+\bar{p}$), while π^0 is reconstructed in the decay to $\gamma\gamma$. Candidate events are required to satisfy the following common selection criteria. The impact parameters of the charged tracks are not limited as the tracks are from secondary vertices. Photons are reconstructed from isolated showers in the EMC. The energy deposited in the nearby TOF counter is included to improve the reconstruction efficiency and energy resolution. Photon energies are required to be greater than 25 MeV in the EMC barrel region ($|\cos\theta| < 0.8$), and greater than 50 MeV in the EMC end caps ($0.86 < |\cos\theta| < 0.92$). The showers in the angular range between the barrel and the end cap are poorly reconstructed and excluded from the analysis. Moreover, the EMC timing of the photon candidate must be in coincidence with collision events, $0 \leq t \leq 700$ ns, to suppress electronic noise and energy deposits unrelated to the events.

A. $\chi_{cJ} \to \Lambda\bar{\Lambda}$

These events contain at least two positively-charged tracks, two negatively-charged tracks and one photon. The Λ ($\bar{\Lambda}$) candidates are reconstructed from pairs of oppositely charged tracks, which are constrained to secondary vertices and have invariant masses closest to the nominal Λ ($\bar{\Lambda}$) mass. The χ^2 of secondary vertex fit must be less than 500. The track information of the secondary vertex is input to the kinematic fit. Here, we take the reconstructed Λ ($\bar{\Lambda}$) as a "virtual" particle [14]. The candidate photons and the two "virtual" particles are subjected to a four constraint (4C) kinematic fit under the hypothesis of $\psi' \to \gamma\Lambda\bar{\Lambda}$ to reduce background and improve the mass resolution. When additional photons are found in an event, all possible combinations are iterated over, and the one with the best kinematic fit χ^2_{4C} is kept. Furthermore, $\chi^2_{4C} < 50$ is required to suppress potential background from $\psi' \to \Sigma^0\bar{\Sigma}^0$. The χ^2_{4C} selection criterion is determined by optimizing the figure of merit (FOM), $FOM = \frac{S}{\sqrt{S+B}}$, where S is the number of signal events from a signal MC simulated sample and B is the number of background events from a background MC simulated sample. Figure 1 (a) shows the comparison of χ^2_{4C} between data and MC simulation, and Fig. 1 (b) shows the scatter plots of $M_{p\pi^-}$ *versus* $M_{\bar{p}\pi^+}$, where a clear $\Lambda\bar{\Lambda}$ signal is seen. The square around the $\Lambda\bar{\Lambda}$ nominal mass with a width of 20 MeV/c^2 is taken as the signal region. The mass window is also optimized by maximizing the FOM. If $N_\gamma \geq 2$, additional selection criteria are applied to suppress backgrounds from $\Sigma^0\bar{\Sigma}^0$ decays. The $\psi' \to \Sigma^0\bar{\Sigma}^0$ candidates can be selected by minimizing $\sqrt{(M_{\gamma\Lambda} - M_{\Sigma^0})^2 + (M_{\gamma\bar{\Lambda}} - M_{\bar{\Sigma}^0})^2}$ in all combinations. However, some background remains in the signal region from $\psi' \to \Sigma^0\bar{\Sigma}^0$ events in which one photon from the Σ^0 decays is not reconstructed. To remove these, events falling into $|M_{\gamma\Lambda} - M_{\Sigma^0}| < 6$ MeV/c^2 and $|M_{\gamma\bar{\Lambda}} - M_{\bar{\Sigma}^0}| <$6 MeV/c^2 have been discarded.

B. $\chi_{cJ} \to \Sigma^0\bar{\Sigma}^0$

The charged track selection and $\Lambda\bar{\Lambda}$ reconstruction are the same as described above for the $\Lambda\ \bar{\Lambda}$. The mass window of Λ ($\bar{\Lambda}$) is optimized to be $|M_{p\pi^-} - 1115.7| < 7$ MeV/c^2 and $|M_{\bar{p}\pi^+} - 1115.7| <$ 7 MeV/c^2. There must be at least three photons in an event. The candidate photons and the two "virtual" particles are subjected to a 4C kinematic fit under the hypothesis of $\psi' \to \gamma\gamma\gamma\Lambda\bar{\Lambda}$ to

reduce background and improve the mass resolution. When additional photons are found in an event, all possible combinations are looped over the one with the smallest kinematic fit χ^2_{4C} is kept, and $\chi^2_{4C} < 35$ is required to suppress the dominant background from $\psi' \to \Sigma^0\bar{\Sigma}^0$. Fig. 1 (c) shows the comparison of χ^2_{4C} between data and MC simulation. The $\Sigma^0\bar{\Sigma}^0$ candidates are chosen by minimizing $\sqrt{(M_{\gamma\Lambda} - M_{\Sigma^0})^2 + (M_{\gamma\bar{\Lambda}} - M_{\bar{\Sigma}^0})^2}$. Fig. 1 (d) shows the scatter plot of $M_{\gamma\Lambda}$ *versus* $M_{\gamma\bar{\Lambda}}$. Clear $\Sigma^0\bar{\Sigma}^0$ signal events can be seen. The square around the $\Sigma^0\bar{\Sigma}^0$ nominal mass with a width of 32 MeV/c^2 is taken as the signal region.

C. $\chi_{cJ} \to \Sigma^+\bar{\Sigma}^-$

These events contain at least one positively-charged, one negatively-charged tracks and five photons. Selecting all combinations of two charged tracks with opposite charge and a group of five photons, we impose a 4C kinematic fit to each combination under the $\psi' \to 5\gamma p\bar{p}$ hypothesis and keep the one with the smallest kinematic fit χ^2_{4C}. $\chi^2_{4C} < 50$ is required to suppress the dominant background from $\psi' \to \Sigma^+\bar{\Sigma}^-$. Fig. 1 (e) shows the comparison of χ^2_{4C} between data and MC simulation. The π^0 candidates are selected by selecting the combination which minimizes $\sqrt{(M^{(1)}_{\gamma\gamma} - M_{\pi^0})^2 + (M^{(2)}_{\gamma\gamma} - M_{\pi^0})^2}$. The $\Sigma^+\bar{\Sigma}^-$ pair is selected by minimizing $\sqrt{(M_{p\pi^0} - M_{\Sigma^+})^2 + (M_{\bar{p}\pi^0} - M_{\bar{\Sigma}^-})^2}$. Fig. 1 (f) shows the scatter plot of $M_{p\pi^0}$ *versus* $M_{\bar{p}\pi^0}$, where clear $\Sigma^+\bar{\Sigma}^-$ signal events can be seen. The square of 1.17 GeV/c^2 $< M_{p\pi^0} <$ 1.20 GeV/c^2 and 1.17 GeV/c^2$< M_{\bar{p}\pi^0} <$ 1.20 GeV/c^2 is taken as the signal region.

IV. BACKGROUND STUDY

A. Continuum backgrounds

The events collected at $E_{cm} = 3.65$ GeV, whose integrated luminosity is more than 1/4 of ψ' samples, are analyzed to measure possible continuum background, and no candidate events remain in the $\Lambda\bar{\Lambda}$, $\Sigma^0\bar{\Sigma}^0$ and $\Sigma^+\bar{\Sigma}^-$ signal regions. Therefore, backgrounds from the continuum are negligible.

B. Dominant backgrounds in $\Lambda\bar{\Lambda}$, $\Sigma^0\bar{\Sigma}^0$ and $\Sigma^+\bar{\Sigma}^-$ final states

By analysing the topology of inclusive simulated events, we find that the dominant remaining backgrounds in $\chi_{cJ} \to \Lambda\bar{\Lambda}$ come from $\psi' \to \Sigma^0\bar{\Sigma}^0$ in which one photon is missing. The non-$\Lambda\bar{\Lambda}$ background from the non-resonant $\chi_{cJ} \to \pi^+\pi^- p\bar{p}$ is negligibly small due to the low efficiency near the mass threshold. In the $\chi_{cJ} \to \Sigma^0\bar{\Sigma}^0$, the dominant backgrounds are also found to arise from $\psi' \to \Sigma^0\bar{\Sigma}^0$. But these backgrounds mainly occur around the ψ' mass. Few background events come from $\psi' \to \pi^0\pi^0 J/\psi$ and $\psi' \to \Xi^0\bar{\Xi}^0$. For $\chi_{cJ} \to \Sigma^+\bar{\Sigma}^-$, the remaining known backgrounds are few. They are $\psi' \to \Sigma^+\bar{\Sigma}^-$, $\psi' \to \pi^0\pi^0 J/\psi$ and $J/\psi \to p\bar{p}$ (or $\gamma p\bar{p}$). Therefore, all non-negligible background events are known and can be estimated by MC simulation according to their branching fractions.

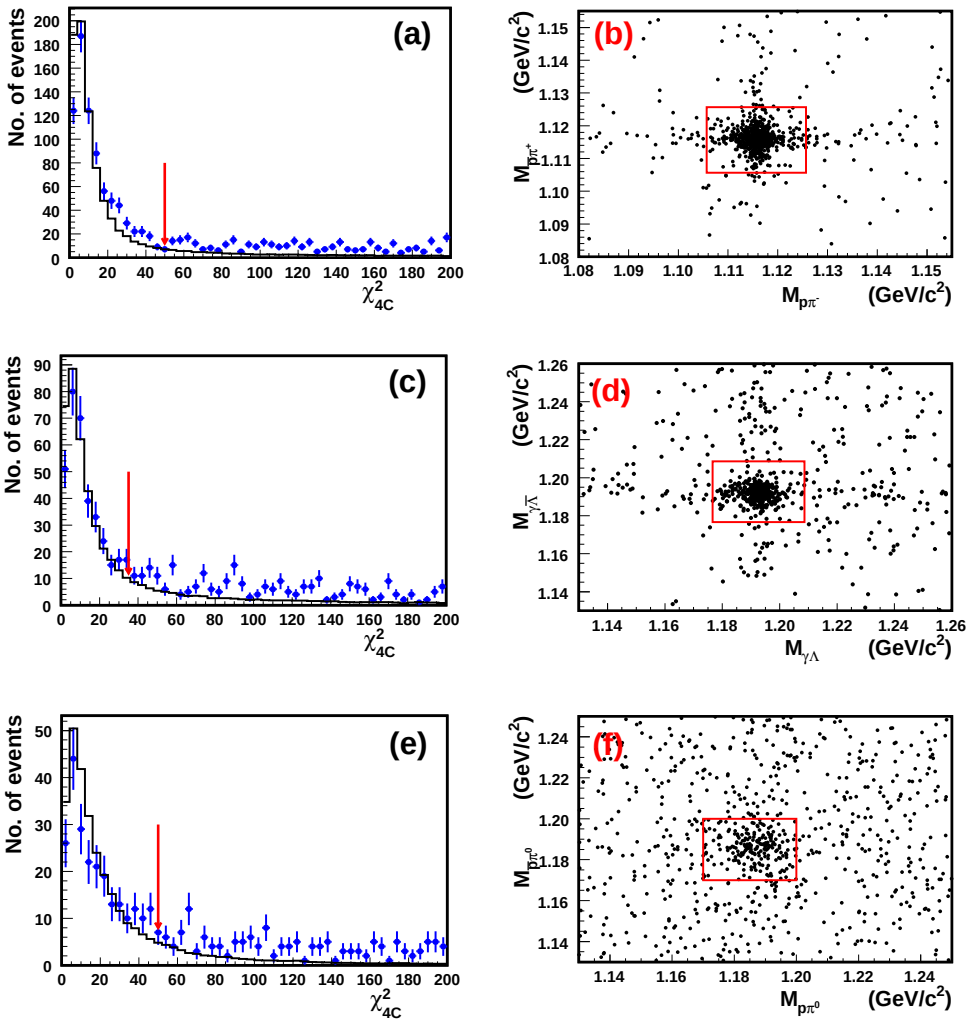

FIG. 1. The χ^2_{4C} $(a,\ c,\ e)$ distributions and scatter plots $(b\ ,d\ ,f)$. Dots with error bars are data, histograms are MC simulation of signal events, where the arrows in Fig. 1 (a), (c) and (e) denote the selection criteria and the rectangles in Fig. 1 (b), (d) and (f) denote the signal regions for the three decays. (a) $\psi' \to \gamma\chi_{cJ}, \chi_{cJ} \to \Lambda\bar{\Lambda}$ candidates, (b) $M_{p\pi^-}$ *versus* $M_{\bar{p}\pi^+}$ in $\gamma\Lambda\bar{\Lambda}$ (data); (c) $\psi' \to \gamma\chi_{cJ}, \chi_{cJ} \to \Sigma^0\bar{\Sigma}^0$ candidates, (d) $M_{\gamma\Lambda}$ *versus* $M_{\gamma\bar{\Lambda}}$ in $\gamma\Sigma^0\bar{\Sigma}^0$ (data); (e) $\psi' \to \gamma\chi_{cJ}, \chi_{cJ} \to \Sigma^+\bar{\Sigma}^-$ events, (f) $M_{p\pi^0}$ *versus* $M_{\bar{p}\pi^0}$ in $\gamma\Sigma^+\bar{\Sigma}^-$ (data).

V. FIT TO THE SIGNAL OF χ_{cJ}

The invariant mass spectra of the baryon pair of all selected events are shown in Figs. 2 (a), (b), and (c) for $\chi_{cJ} \to \Lambda\bar{\Lambda},\ \Sigma^0\bar{\Sigma}^0$ and $\Sigma^+\bar{\Sigma}^-$, respectively. Clear $\chi_{c0,1,2}$ signals can be seen in $\Lambda\bar{\Lambda}$, and a clean χ_{c0} signal is seen in both $\Sigma^0\bar{\Sigma}^0$ and $\Sigma^+\bar{\Sigma}^-$, but for $\chi_{c1,2}$ signals are not clear enough in $\Sigma^0\bar{\Sigma}^0$ and $\Sigma^+\bar{\Sigma}^-$. We fit the invariant mass spectra of baryon pairs, $M_{B\bar{B}}$, to extract the numbers of χ_{cJ} signal events, where the signal function is taken from Breit-Wigner functions convolved with the Crystal Ball (CB) function to describe detector resolution, a 2^{nd} order Chebychev polynomial is used to describe non-peaking backgrounds, and the dominant background events, estimated by

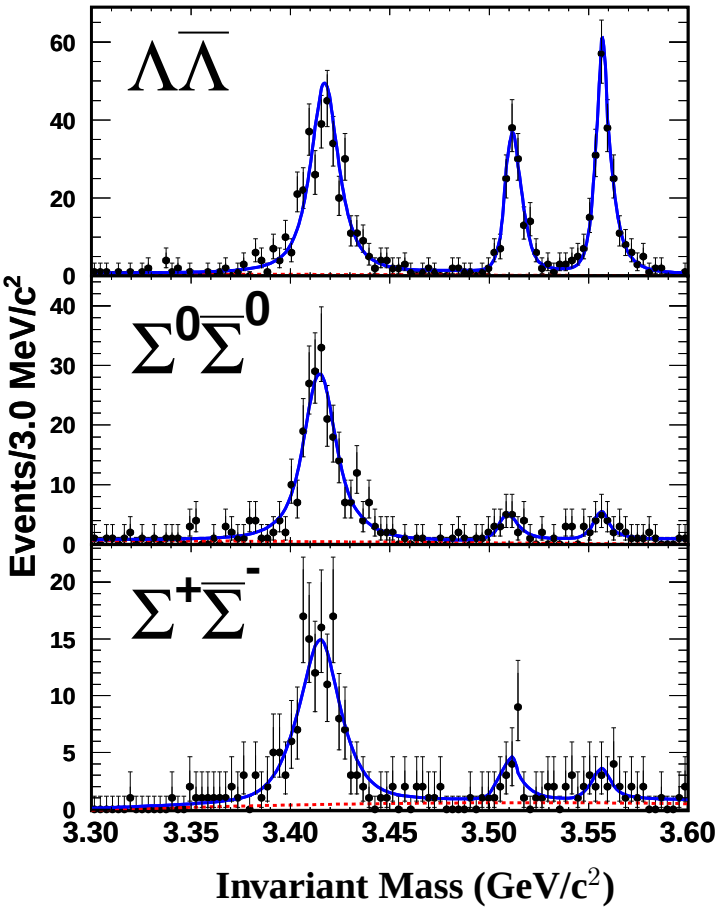

FIG. 2. The fit to the χ_{cJ} signal. Dots with error bars are data. The solid line is the fit to the signal. The dashed-line is other background.

MC simulation, have been directly subtracted from data. The widths of the Breit-Wigner functions were fixed according to the PDG [6], the parameters in CB function are fixed to their values obtained from a fit to MC simulation, and these parameters are varied within their errors for the determination of systematic uncertainties. The $\chi^2/d.o.f$ are 0.507, 0.344, and 0.326 for $\Lambda\bar{\Lambda}$, $\Sigma^0\bar{\Sigma}^0$, and $\Sigma^+\bar{\Sigma}^-$, respectively. The numbers of $\chi_{c0,1,2}$ signal events from fits are listed in Table I. For the signal of $\chi_{c1,2}$ in $\Sigma^0\bar{\Sigma}^0$ and $\Sigma^+\bar{\Sigma}^-$ channels, upper limits at the 90% C.L. are also determined with a Bayesian method [15]. The statistical significances of signals are calculated as $\sqrt{-2\Delta\ln\mathcal{L}}$, where $\Delta\ln\mathcal{L}$ is the difference between the logarithmic maximum likelihood (ML) values of the fit with and without the corresponding signal function. They are 4.3σ and 4.6σ for $\chi_{c1,2}\to\Sigma^0\bar{\Sigma}^0$, and 4.4$\sigma$ and 3.0σ for $\chi_{c1,2}\to\Sigma^+\bar{\Sigma}^-$, respectively. Table I also lists the signal efficiencies which are obtained from MC simulation. Here, the proper angular distributions for photons emitted in $\psi'\to\gamma\chi_{cJ}$ are used [16]. The decay of $\chi_{cJ}\to B\bar{B}$ and the decay of baryons are generated with a phase space model.

TABLE I. Efficiencies (ϵ in $\%$) obtained from analysis of MC generated events, and the yields N^{obs} found in data.

Mode	χ_{c0}		χ_{c1}		χ_{c2}	
	N^{obs}	ϵ	N^{obs}	ϵ	N^{obs}	ϵ
$\Lambda\bar{\Lambda}$	368.9±22.1	26.6	135.6±12.6	27.9	207.1±15.7	26.3
$\Sigma^0\bar{\Sigma}^0$	242.8±17.1	12.2	20.0±5.3	13.2	18.9±5.3	12.7
$\Sigma^+\bar{\Sigma}^-$	147.8±13.8	12.3	18.0±5.4	13.1	14.5±5.6	12.3

VI. SYSTEMATIC ERROR

The systematic errors originate from the uncertainties of the tracking efficiency, $\Lambda, \bar{\Lambda}$ combined efficiency for tracking and reconstruction, 4C kinematic fit, the photon efficiency, the uncertainty of the branching fractions of the intermediate states (from PDG [6]), the uncertainty of fit range, the uncertainty of the angular distribution of $\chi_{c1,c2} \to B\bar{B}$, background shape, signal lineshape MC resolution and the uncertainty for the total number of ψ' events.

1. The control sample $\psi' \to \Lambda\bar{\Lambda}$ is employed to study the combined efficiency for tracking and reconstruction of Λ $(\bar{\Lambda})$. Taking the Λ as an example, the selection criteria of charged tracks are the same as before except to use particle identification information to suppress the background; at least one positively-charged and one negatively-charged tracks are selected and required to be identified as a π^+ track and an anti-proton track. Also, the invariant mass of $\pi^+\bar{p}$ is required to be within 10 MeV/c^2 of the nominal $\bar{\Lambda}$ mass; these events are taken as $\bar{\Lambda}$ candidates. Furthermore, the momentum of $\bar{\Lambda}$ candidates is required to be within 20 MeV/c of its nominal value in two-body decay of $\psi' \to \Lambda\bar{\Lambda}$. The number of Λ signal events, N^0_Λ, is extracted by fitting the recoiling mass spectrum of $\bar{\Lambda}$, $M^{\bar{\Lambda}}_{recoil}$. Then two additional charged tracks, a π^- and a proton, are required to reconstruct Λ. The number of Λ signal events, N^1_Λ, is extracted by fitting $M^{\bar{\Lambda}}_{recoil}$ after requiring the Λ to be reconstructed. The combined efficiency of tracking and reconstruction for Λ is determined as $\epsilon_\Lambda = \frac{N^1_\Lambda}{N^0_\Lambda}$. Similarly, the combined efficiency of tracking and reconstruction for $\bar{\Lambda}$ are obtained. The difference of efficiencies between data and MC simulation are taken as the systematic error due to Λ $(\bar{\Lambda})$ tracking and reconstruction, and they are found to be 2.0% for a Λ and 5.0% for a $\bar{\Lambda}$.

2. From the very clean $J/\psi \to \pi^+\pi^- p\bar{p}$ control sample, the MDC tracking efficiency for MC simulated events agrees with that determined using data to within 1% for each charged track. Hence, 2% is taken as the systematic error for the $\Sigma^+\bar{\Sigma}^-$ final state.

3. The uncertainty due to photon detection efficiency is 1% per photon, which is determined from the control sample $J/\psi \to \rho\pi$ [17].

4. Five control samples, $J/\psi \to \Lambda\bar{\Lambda}, J/\psi \to \Sigma^0\bar{\Sigma}^0, J/\psi \to \Xi^0\bar{\Xi}^0, \psi' \to \pi^0\pi^0 J/\psi$ ($J/\psi \to p\bar{p}$) and $\psi' \to \pi^0\pi^0 J/\psi(J/\psi \to p\bar{p}\pi^0)$ are used to study the efficiencies of the 4C kinematic fits for the signal channels. The signal events are selected in data and inclusive MC events without 4C fit information. The remaining background is found to be negligible according to the topology analysis with inclusive MC events. The number of signal events is taken as N_0, and the number of surviving the 4C kinematic fit are taken as N_1. The efficiency of the 4-C fit is $\frac{N_1}{N_0}$. The difference between data and MC is taken as the systematic error due to

the 4C fit. For $\Lambda\bar{\Lambda}$, where the final state is $\psi' \to \gamma\Lambda\bar{\Lambda}$, two control samples, $J/\psi \to \Lambda\bar{\Lambda}$, and $J/\psi \to \Sigma^0\bar{\Sigma}^0$, are used to investigate the error from 4C fit. The final states in these two control samples contain one photon less or more than the signal channel. Conservatively, the larger difference observed in the two control samples, 2.4%, is taken as the final error. Similarly, the larger difference in $J/\psi \to \Sigma^0\bar{\Sigma}^0$ and $J/\psi \to \Xi^0\bar{\Xi}^0$, 2.9%, is taken as the error of the $\chi_{cJ} \to \Sigma^0\bar{\Sigma}^0$ channel, and the larger in $\psi' \to \pi^0\pi^0 J/\psi$ ($J/\psi \to p\bar{p}$) and $\psi' \to \pi^0\pi^0 J/\psi$ ($J/\psi \to p\bar{p}\pi^0$), 1.3%, is taken as the error of $\chi_{cJ} \to \Sigma^+\bar{\Sigma}^-$.

5. When changing mass ranges in fitting $M_{B\bar{B}}$ signals from 3.32 GeV/c^2 to 3.6 GeV/c^2, 3.25 GeV/c^2 to 3.62 GeV/c^2 and 3.3 GeV/c^2 to 3.62 GeV/c^2, it is observed that there are some differences on the fitted numbers of signal events. The biggest differences between data and MC simulation are taken as the systematic errors due to the uncertainty of fitting range.

6. The signal function in fitting $M_{B\bar{B}}$ invariant mass is taken as the parameterized shape from MC simulated channels in which the widths of χ_{cJ} are fixed since we only observe a small number of signal events in $\chi_{c1,2} \to \Sigma^0\bar{\Sigma}^0$ and $\Sigma^+\bar{\Sigma}^-$. Therefore, there can not be too many free parameters. When changing the parameters of χ_{cJ} widths within 1σ, it is found that the difference of the numbers of fitted $\chi_{c1,2}$ events between data and MC is 1.2%, 0.0%, 0.0% for $\Lambda\bar{\Lambda}$, 1.9%, 0.0%, 3.7% for $\Sigma^0\bar{\Sigma}^0$ and 1.0%, 0.5%, 2.0% for $\Sigma^+\bar{\Sigma}^-$. Hence, we take the difference as the systematic error due to χ_{cJ} widths.

7. The partial width for an E1/M1 radiative transition is proportional to the cube of the radiative photon energy (E_γ^3), which leads to a diverging tail in the lower mass region. Two damping functions have been proposed by the KEDR [18] and the CLEO [19] collaborations and have been used in addition to the standard approach in the formula describing the fit to the signal lineshape. Differences with respect to the fit not taking into account this damping factor are observed, and the greater of the two differences is taken as the systematic uncertainty associated with the signal lineshape.

8. From the $J/\psi \to \Lambda\bar{\Lambda}$ control sample, it is found that the resolution is different for data and MC. Therefore, it is necessary to consider the difference in fitting the χ_{cJ} signal between fixing and floating the MC parameter. Conservatively, we take 1.5%, 0.5% and 2.4% as the systematic errors for the MC resolution for the $\Lambda\bar{\Lambda}$ final states. However, from the the control samples $J/\psi \to \Sigma^0\bar{\Sigma}^0$ and $J/\psi \to \Xi^0\bar{\Xi}^0$, it is found that data and MC are consistent. Therefore, the systematic errors of MC resolution in $\Sigma^0\bar{\Sigma}^0$ and $\Sigma^+\bar{\Sigma}^-$ final state are negligible.

9. To estimate the uncertainty of the angular distribution, we use another model in which the angular distribution of $\chi_{c1,2} \to B\bar{B}$ is taken into account according to the helicity amplitude [20] and then take the biggest difference as the systematic error of the angular distribution.

10. In Fig. 2, the combinatorial background curves are fitted with a 2^{nd} order Chebychev polynomial. The background function is changed to 1^{st} and 3^{rd} order polynomials, and the largest difference is taken as the systematic error due to the uncertainty in the description of the background shape.

11. The total number of ψ' events are obtained by studying inclusive hadronic ψ' decays with uncertainty of 0.81% [7].

Table II lists all systematic error contributions, and the total systematic error is obtained by adding the individual contributions in quadrature.

TABLE II. Systematic errors in the branching fraction measurements (%)

.

	$\chi_{cJ} \to \Lambda\bar{\Lambda}$			$\chi_{cJ} \to \Sigma^0\bar{\Sigma}^0$			$\chi_{cJ} \to \Sigma^+\bar{\Sigma}^-$		
Source	χ_{c0}	χ_{c1}	χ_{c2}	χ_{c0}	χ_{c1}	χ_{c2}	χ_{c0}	χ_{c1}	χ_{c2}
The total number of ψ'	0.81	0.81	0.81	0.81	0.81	0.81	0.81	0.81	0.81
MDC tracking $(p, \bar{p})$	–	–	–	–	–	–	2.0	2.0	2.0
Photon efficiency	1.0	1.0	1.0	3.0	3.0	3.0	5.0	5.0	5.0
Λ reconstruction	2.0	2.0	2.0	2.0	2.0	2.0	–	–	–
$\bar{\Lambda}$ reconstruction	5.0	5.0	5.0	5.0	5.0	5.0	–	–	–
Kinematic fit	2.4	2.4	2.4	2.9	2.9	2.9	1.3	1.3	1.3
Fitting range	2.7	3.6	4.3	1.4	6.7	4.3	1.4	3.0	7.2
χ_{cJ} width	1.2	0.0	0.0	1.9	0.0	3.7	1.0	0.5	2.0
Angular distribution	0.0	3.2	6.0	0.0	3.2	6.0	0.0	3.2	6.0
Background shape	0.5	1.3	1.3	1.7	7.8	6.0	1.8	2.5	3.0
Signal lineshape	0.7	2.1	2.7	1.4	1.0	2.2	0.0	2.7	5.5
MC resolution	1.5	0.5	2.4	0.0	0.0	0.0	0.0	0.0	0.0
B($\psi' \to \gamma\chi_{cJ}$)	3.2	4.3	4.0	3.2	4.3	4.0	3.2	4.3	4.0
B($\Sigma \to \pi^0 p$)	–	–	–	–	–	–	0.82	0.82	0.82
B($\Lambda \to p\pi$)	1.1	1.1	1.1	1.1	1.1	1.1	–	–	–
Total systematic error	7.7	9.3	11.1	8.3	13.6	13.2	7.0	9.1	13.4

VII. RESULTS

The branching fraction of $\chi_{cJ} \to B\bar{B}$ is determined by

$$\mathcal{B}(\chi_{cJ} \to B\bar{B}) = \frac{N^{obs}[\chi_{cJ}]}{N_{\psi'} \cdot \epsilon \cdot \prod_i \mathcal{B}_i},$$

and if the signal is not significant, the corresponding upper limit of branching fraction is set with

$$\mathcal{B}(\chi_{cJ} \to B\bar{B}) < \frac{N^{obs}_{UL}[\chi_{cJ}]}{N_{\psi'} \cdot \epsilon \cdot \prod_i \mathcal{B}_i \cdot (1.0 - \sigma_{sys.})},$$

where, N^{obs} is the number of observed signal events and N^{obs}_{UL} is the upper limit of the number of events, ϵ is the detection efficiency shown in Table I, $\sigma_{sys.}$ is the relative the systematic error, $N_{\psi'}$ is the total number of ψ' events [7], and $\prod_i \mathcal{B}_i$ is the product of the branching fractions taken from PDG [6] for $\psi' \to \gamma\chi_{cJ}$ and the other decays that are involved. With the numbers listed in Table I and the branching fractions for the relevant baryon decays, the branching fractions or the upper limits at the 90% C.L. for χ_{cJ} decays are determined, as listed in Table III.

TABLE III. Branching fractions (or their upper limits) of $\chi_{cJ} \to \Lambda\bar{\Lambda}, \Sigma^0\bar{\Sigma}^0$ and $\Sigma^+\bar{\Sigma}^-$ (in units of 10^{-5}). The first error is statistical and the second is systematic.

Mode		χ_{c0}	χ_{c1}	χ_{c2}
$\Lambda\bar{\Lambda}$	This work	33.3±2.0±2.6	12.2±1.1±1.1	20.8±1.6±2.3
	PDG	33.0±4.0	11.8±1.9	18.6±2.7
	CLEO	33.8± 3.6±2.2±1.7	11.6±1.8±0.7±0.7	17.0±2.2±1.1±1.1
	Theory	$(93.5 \pm 20.5^a, 22.1 \pm 6.1^b)$[21]	–	$(15.2 \pm 1.7^a, 4.3 \pm 0.6^b)$[21]
		11.9∼15.1[23]	3.9[22]	3.5[22]
$\Sigma^0\bar{\Sigma}^0$	This work	47.8±3.4±3.9	3.8±1.0±0.5 (< 6.2)	4.0±1.1±0.5 (< 6.5)
	PDG	42.0±7.0	<4.0	<8.0
	CLEO	44.1±5.6±4.2±2.2	<4.4	<7.5
	Theory	$(25.1 \pm 3.4^a, 18.7 \pm 4.5^b)$[21]	–	$(38.9 \pm 8.8^a, 4.2 \pm 0.5^b)$[21]
		–	3.3[22]	5.0[22]
$\Sigma^+\bar{\Sigma}^-$	This work	45.4±4.2±3.0	5.4±1.5±0.5 (< 8.7)	4.9±1.9±0.7 (<8.8)
	PDG	31.0±7.0	<6.0	<7.0
	CLEO	32.5±5.7±4.0±1.7	<6.5	<6.7
	Theory	5.5 ∼ 6.9[23]	3.3[22]	5.0[22]

VIII. SUMMARY

Three two-body decay modes of χ_{cJ} into pairs of baryons are observed, and their branching fractions are measured at BESIII. The significances for $\chi_{c1,2}$ in $\Sigma^0\bar{\Sigma}^0$ and $\Sigma^+\bar{\Sigma}^-$ final states are improved relative to the CLEO [4] collaboration. For the decay of $\chi_{cJ} \to \Lambda\bar{\Lambda}$, the experimental results are not consistent with theoretical predictions [21–23] within errors. For the decays of $\chi_{c1,2} \to \Sigma^0\bar{\Sigma}^0$ and $\Sigma^+\bar{\Sigma}^-$, comparisons between experiments and theoretical predictions are inconclusive due to the limited experimental precision.

IX. ACKNOWLEDGEMENT

The BESIII collaboration thanks the staff of BEPCII and the computing center for their hard efforts. This work is supported in part by the Ministry of Science and Technology of China under Contract No. 2009CB825200, 2009CB825206; National Natural Science Foundation of China (NSFC) under Contracts Nos. 10625524, 10821063, 10825524, 10835001, 10935007, 10975143, 10975047, 10979008, 11125525, 11275057; Joint Funds of the National Natural Science Foundation of China under Contracts Nos. 11079008, 11079027, 11179007; the Chinese Academy of Sciences (CAS) Large-Scale Scientific Facility Program; CAS under Contracts Nos. KJCX2-YW-N29, KJCX2-YW-N45; 100 Talents Program of CAS; Istituto Nazionale di Fisica Nucleare, Italy; Ministry of Development of Turkey under Contract No. DPT2006K-120470; U. S. Department of Energy under Contracts Nos. DE-FG02-04ER41291, DE-FG02-91ER40682, DE-FG02-94ER40823; U.S. National Science Foundation; University of Groningen (RuG) and the Helmholtzzentrum fuer Schwerionenforschung GmbH (GSI), Darmstadt; WCU Program of Na-

tional Research Foundation of Korea under Contract No. R32-2008-000-10155-0.

[1] G. T. Bodwin, E. Braaten and G. P. Lepage, Phys. Rev. D **51**, 1125 (1995).
[2] J. Z. Bai *et al.* (BES Collaboration), Phys. Rev. D **67**, 112001 (2003).
[3] M. Ablikim *et al.* (BES Collaboration), Phys. Rev. D **73**, 052006 (2006).
[4] P. Naik *et al.* (CLEO Collaboration), Phys. Rev. D **78**, 031101 (2008).
[5] S. J. Brodsky and G. P. Lepage, Phys. Rev. D **24**, 2848 (1981).
[6] K. Nakamura *et al.* (Particle Data Group), J. Phys. G **37**, 075021 (2012).
[7] M. Ablikim *et al.* (BESIII Collaboration), arXiv:1209.6199 [hep-ex].
[8] M. Ablikim *et al.* (BESIII Collaboration), Nucl. Instrum. Meth. A **614**, 345 (2010).
[9] S. Agostinelli *et al.* (GEANT4 Collaboration), Nucl. Instrum. Meth. A **506**, 250 (2003).
[10] J. Allison *et al.*, IEEE Trans. Nucl. Sci. **53**, 270 (2006).
[11] S. Jadach, B. F. L. Ward and Z. Was, Comput. Phys. Commun. **130**, 260 (2000),
S. Jadach, B. F. L. Ward and Z. Was, Phys. Rev. D **63**, 113009 (2001).
[12] R. G. Ping *et al.*, Chinese Physics C **32**, 599 (2008).
[13] J. C. Chen *et al.*, Phys. Rev. D **62**, 034003 (2000).
[14] M. Xu $et\ al.$, Chinese Physics C **33**, 428 (2009).
[15] Y. S. Zhu, $et\ al.$, Chinese Physics C **32**, 363 (2008).
[16] W. M. Tanenbaum *et al.*, Phys. Rev. D **17**, 1731 (1978),
G. Karl, S. Meshkov and J. L. Rosner, Phys. Rev. D **13**, 1203 (1976),
M. Oreglia *et al.*, Phys. Rev. D **25**, 2259 (1982).
[17] M. Ablikim $et\ al.$ (BESIII Collaboration), Phys. Rev. D **83**, 11205 (2011).
[18] V. V. Anashin *et al.* (KEDR Collaboration), arXiv:1012.1694 [hep-ex].
[19] R. E. Mitchell *et al.* (CLEO Collaboration), Phys. Rev. Lett. **102**, 011801 (2009).
[20] G. R. Liao, R. G. Ping and Y. X. Yang, Chin. Phys. Lett. **26**, 051101 (2009).
[21] R. G. Ping, B. S. Zou and H. C. Chiang, Eur. Phys. J. A **23**, 129 (2004).
[22] S. M. H. Wong, Eur. Phys. J. C **14**, 643 (2000).
[23] X. H. Liu and Q. Zhao, J. Phys. G G**38**, 035007 (2011).